A LIGHTWEIGHT UNIVERSAL GRIPPER WITH LOW ACTIVATION FORCE FOR AERIAL GRASPING

A PREPRINT

Paul Kremer[*] ✉
p.kremer@uni.lu

Hamed Rahimi Nohooji[†]
hamed.rahimi@uni.lu

Jose Luis Sanchez-Lopez[†]
joseluis.sanchezlopez@uni.lu

Holger Voos[*] [†]
holger.voos@uni.lu

October 11, 2022

ABSTRACT

Soft robotic grippers have numerous advantages that address challenges in dynamic aerial grasping. Typical multi-fingered soft grippers recently showcased for aerial grasping are highly dependent on the direction of the target object for successful grasping. This study pushes the boundaries of dynamic aerial grasping by developing an omnidirectional system for autonomous aerial manipulation. In particular, the paper investigates the design, fabrication, and experimental verification of a novel, highly integrated, modular, sensor-rich, universal jamming gripper specifically designed for aerial applications. Leveraging recent developments in particle jamming and soft granular materials, the presented gripper produces a substantial holding force while being very lightweight, energy-efficient and only requiring a low activation force. We show that the holding force can be improved by up to $50\,\%$ by adding an additive to the membrane's silicone mixture. The experiments show that our lightweight gripper can develop up to $15\,\mathrm{N}$ of holding force with an activation force as low as $2.5\,\mathrm{N}$, even without geometric interlocking. Finally, a pick and release task is performed under real-world conditions by mounting the gripper onto a multi-copter. The developed aerial grasping system features many useful properties, such as resilience and robustness to collisions and the inherent passive compliance which decouples the UAV from the environment.

Keywords universal jamming gripper · aerial manipulation · soft gripper · soft aerial robotics

License

Funding

This project was partially supported by the European Commission Horizon2020 research and innovation programme, under the grant agreement No 101017258 (SESAME) and by the Luxembourg National Research Fund (FNR) 5G-SKY project (ref. C19/IS/113713801).

[*]University of Luxembourg, Faculty of Science, Technology and Medicine (FSTM), 2, Av. de l'Université, L-4365 Esch-sur-Alzette, Luxembourg

[†]Interdisciplinary Center for Security, Reliability and Trust (SnT), University of Luxembourg, 29, Av. J.F. Kennedy, L-1855 Luxembourg

1 Introduction

During the last decade, Unmanned Aerial Vehicles (UAVs) attracted considerable research interest from the robotics community. In 2010 seminal work on fully functional UAVs for plant inspection for UK onshore oil refineries [36] was developed. Only a few years later, UAV technology had matured to a point where it could be utilized in several applications such as remote sensing and monitoring of forest fires [8], agricultural products [11], border monitoring [3], search and rescue [1], plant assets inspection [10], and transmission line inspection [24]. Despite the advantages of UAVs with regard to sensing and monitoring the environment, such systems fall short when it comes to the physical interaction with their surroundings. Consequently, the field of aerial manipulation emerged, addressing those deficits by equipping UAVs with robotic manipulators [6] and claw-like grippers [33], [23]. In the last few years, aerial manipulation has considerably evolved, featuring numerous applications, including medical goods delivery [37], infrastructure monitoring and maintenance [5], autonomous transportation and construction [27], agriculture [32], forestry [19], and autonomous charging via perching [30].

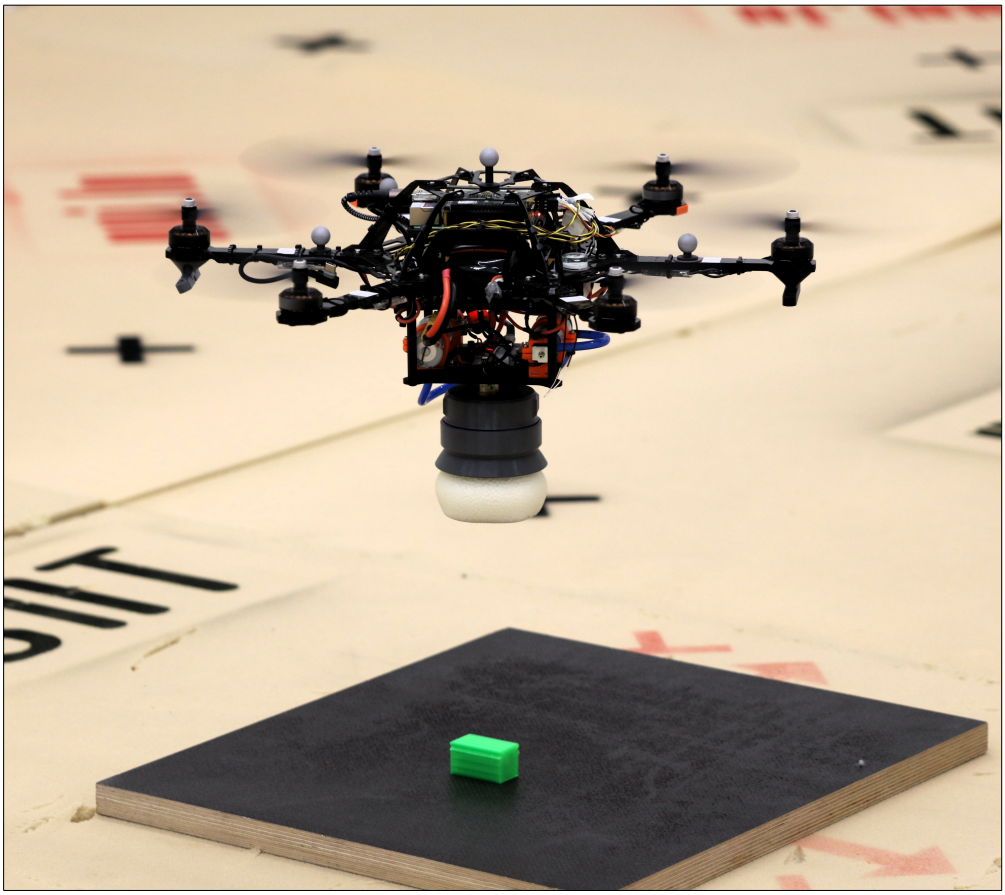

Figure 1: General aerial grasping concept. Our compact universal gripper is attached to the UAV's cargo bay, similar to a claw-gripper. The UAV's landing gear has been removed as this functionality is assured by the gripper. The box (green) serves as the dummy payload.

Recently, the field of aerial manipulation has seen a push towards soft robotics. In contrast to traditional rigid robotic grippers, soft grippers passively conform to the grasped object, enabling tolerance to imprecisions [35] while also being passively compliant, adapting to the complex environments they interact with. They generally possess very favorable properties when grasping complex geometries in unstructured environments. Several soft grippers were developed over the last decade, e.g., pneumatic soft fingers [9], [21], origami grippers [25], suction grippers [20], and tendon grippers [28].

Despite the great potential of soft grippers as a lightweight and compliant alternative for aerial manipulation, little attempt was made to explicitly design and model continuously deformable, soft grasping structures in the aerial context. Soft grippers in aerial robotics, where the UAV system has to safely interact with its environment and with humans,

have a vast range of applications, e.g., object grasping [29], perching [13], or pipe inspection [15]. Recently, the design and control of a soft aerial robot, consisting of a quadrotor and a tendon-actuated soft gripper was investigated. A decoupled control approach for the quadrotor and the soft gripper was derived, combining a geometric controller and a minimum-snap trajectory optimization for the quadrotor (rigid) base, with a quasi-static finite element model and control-space interpolation for the soft gripper [12], [14]. A quadrotor platform combined with a custom *Fin Ray* gripper was presented in [2] that uses semi-flexible jaws which increase the contact surface between the gripper and the payload.

In [7] a different type of soft gripper was introduced based on the jamming principle of certain granular materials. This Universal Gripper (UG), being just a simple bag containing granular material, works via three distinct mechanisms that are involved in the grasping process, namely geometric interlock F_G, suction F_S and friction F_R, which all come into play once the soft membrane of the gripper is pressed against the targeted object by a force called *activation force*. After jamming (hardening) of the granular material [4], the resulting *holding force* is then the sum of the different components $F_H = F_G + F_S + F_R$. The jamming typically involves creating a vacuum inside the membrane, however, other jamming principles exist, e.g., magnetically [31], or hydraulically [34]. UGs have virtually infinite degrees of freedom that do not need to be controlled explicitly.

This work is the first study that employs a universal jamming gripper in aerial manipulation. We provide a design and implementation of such a gripper with pneumatic actuation in a small and compact form factor, suitable for small to medium-sized multicopters. The goal is to address some of the open challenges, particularly with regard to grasping in unstructured environments, where only very few assumptions can be made about the shape, size, and weight of the targeted object. This paper shows that due to their simple construction, UGs are easy and cheap to build and offer distinct advantages, especially in the context of aerial manipulation. This work paves the way toward unlocking a variety of practical applications in the context of aerial grasping. The developed soft gripper is experimentally validated in a simple pick & release task under lab conditions, see Fig. 1.

The main contributions of this work are as follows:

1. To the best of our knowledge, despite having excellent grasping properties in unstructured environments, there is currently no work that discusses the usage of UGs in aerial manipulation. UGs can relax the aerial vehicle's dependence on the grasping direction and address open aerial grasping challenges concerning robustness to object geometry and grasping accuracy.
2. For optimal performance in aerial grasping, we specifically designed our UG to be as lightweight as possible. Differing from previous grippers like [18], or [16] which require a high activation force, the presented gripper is able to work with a much lower activation force that is more suitable for aerial grasping. The developed gripper's holding force is improved by using soft filler particles [17]. We show that we can further increase the grasping force by using a silicone additive.
3. Compared with available soft grippers for aerial grasping [13], [2], the proposed design has many advantages, such as resilience and robustness to collisions and the inherent passive compliance which decouples the UAV from the environment. However, the salient feature of the proposed system lies in the intuitiveness of the design in the context of aerial grasping and in the simplicity of its grasping mechanism. Moreover, the resultant grasping system is modular, energy-efficient, and highly integrated while being structurally simple and inexpensive to fabricate.
4. We provide extensive experimental validation of our design in conjunction with our custom test jig. Using our experimental data, we then propose a digital twin of our UG. Moreover, we show our UG attached to a multicopter, performing a pick and release task, validating the overall concept.

The rest of this work is organized as follows. Section 2 introduces the main design challenges and our solutions associated with the design and manufacturing of a lightweight UG in an aerial context. The presented gripper is then validated experimentally in Section 3, where we also present our findings with regard to the minimum activation force and the impact of the silicone additive on the holding force. Based on those results, we propose a digital twin of our UG in Section 4. We then showcase our UG in an aerial application in Section 5, and we discuss our design and findings in Section 6. We conclude this work in Section 7 by summarizing our main findings and indicating future work planned in this context.

2 Concept and System Architecture

In this section, we first introduce the general concept of our UG and the associated design challenges in the context of aerial manipulation. We then take an in-depth look at the electro-mechanical, pneumatic, and software components.

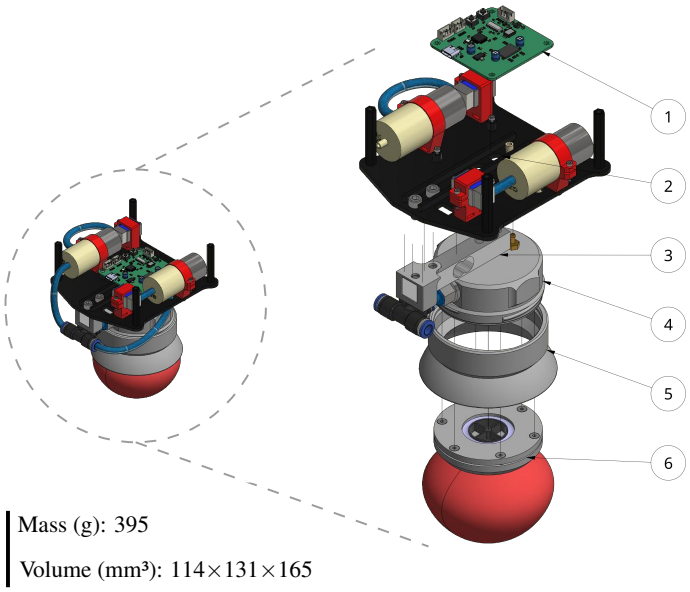

Figure 2: Complete assembly of the grasping system. ① Controller board, ② Base assembly with pneumatic system, ③ Load-cell, ④ Gripper-floor, ⑤ Wedge with thread, ⑥ Membrane module

2.1 Concept

Multirotor platforms come with many benefits, but also with a set of limitations. The most relevant ones are their limited payload capability, the constrained volume for attachments, their underactuated nature, and the challenging dynamics coupling. The dynamics coupling is particularly important for aerial systems carrying manipulators [22], but it also poses a problem for simpler 'claw' setups where only the grasping element gets in contact with the environment. Elastic elements inserted in the construction of the grasping device efficiently reduce the dynamic coupling by softening the hard socks associated with typical grasping operations. Those elastic elements are inherently present in UGs as represented by their soft membrane. UGs are thus an ideal fit, provided they can be constructed to fit the size and weight envelope of aerial platforms.

Our proof-of-concept aerial platform is a medium-sized, modified *Asctec Firefly* hexacopter with a wheelbase of $430\,\mathrm{mm}$, and a maximum payload capacity of $1\,\mathrm{kg}$. This air-frame conveniently features a cargo bay measuring $120\,\mathrm{mm} \times 120\,\mathrm{mm}$, which we use as the anchor point for our gripper. This particular mounting scheme with the gripper oriented towards the bottom is commonly referred to as a 'claw'.

Compatibility with state-of-the-art autopilots (e.g., Pixhawk) is assured by either directly connecting the gripper to the autopilot via UART or by connecting it to the corresponding companion computer using USB. For ease of integration, our concept envisions being directly powered by the UAV's main 3S-4S battery, which eliminates carrying an additional battery. Lightweight construction, modularity, and tight integration of the electronics, the sensors, and the software are the driving concepts of our design.

To make our work easily reproducible, accessible, and low-cost (<$100, without the equipment), we limited our design to widely available and inexpensive manufacturing techniques, where a Fused Deposition Modeling (FDM) printer and a high-power single-stage vacuum pump represent the bulk of the cost. Furthermore, we designed our grasper around widely available off-the-shelf parts.

The complete grasping system is detailed in Fig. 2. Its major subsystems are explained hereafter.

2.2 Pneumatics and Mechanics

The role of the pneumatic system is twofold: 1. to pressurize the membrane and thus allow the contained granular material to flow easily within the free, air-filled volume; 2. to vaccumize the membrane and consequently jam (i.e., solidify) the granular material.

UGs can be realized in two distinguishable topologies; as closed-loop or open-loop systems. In closed-loop systems, the fluid surrounding the granular material stays contained within the system. An example of such a system is the

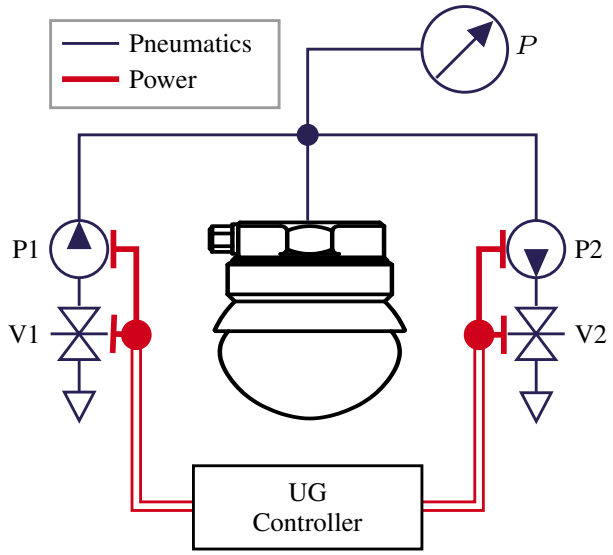

Figure 3: Pneumatic system. The jamming gripper is fed by two pumps. Pump P1 will inflate the balloon, fluidizing its content. Pump P2 is used to create a vacuum strong enough to jam the particles inside the balloon. The solenoid valves V1, V2 are required to prevent air from leaking through the inactive pumps. All pneumatic components are actuated based on the control inputs from the main controller.

magnetorheological fluid-based UG shown in [31] for the hydraulic UG presented in [34]. Generally, these systems have the distinct disadvantage that the fluid has to stay contained within the system (e.g., in tanks that add weight and cost) and that leakage must be considered as a critical failure mode. On the other hand, open-loop systems exchange their fluid with their environment. Their operating fluid is thus typically air, resp. water for underwater applications [26]. Those systems have the distinct advantage that their fluid is abundantly present in their surroundings, which eliminates the storage needs and reduces the severity of leakage and even membrane rupture. Open-loop systems are generally better suited for lightweight construction and require less engineering effort.

Therefore, the pneumatic system presented in this paper (Fig. 3) has an open-loop structure and uses air as its operating fluid. It consists of two small, non-reversible diaphragm pumps (P1, P2) coupled to two pneumatic solenoid 2/1-way valves (V1, V2). The air pressure in the system is measured by the Microelectromechanical System (MEMS) pressure sensor P. This particular setup is very low cost and has a favorable mass distribution due to symmetry. By design, diaphragm pumps act as one-way check-valves, not restricting the airflow in their nominal direction, which therefore requires closing the valve associated with the antagonistic pump such that they can establish a pressure differential. This particular topology also permits to completely seal the system, keeping the membrane pressurized (resp. in a state of vacuum) without powering the pumps, thus saving energy.

We utilize two 12V, 7 W, `SC3704PM` diaphragm pumps rated for a pressure differential of $46\,\mathrm{kPa}$ at $2\,\mathrm{L\,min^{-1}}$. The miniature 2/1 air valves are of type `SCO520FVG`. Our pneumatic system is therefore very low power (typically $<10\,\mathrm{W}$) contrary to other systems frequently featured in the literature, which are using heavy ($>1\,\mathrm{kg}$) stationary, high-power vacuum pumps in the $500\,\mathrm{W}$ range and reaching pressure differentials beyond $80\,\mathrm{kPa}$ [7], [17]. Note that our lower-power system naturally comes with longer cycle times and a lower maximum pressure differential, in practice, approximately $28\,\mathrm{kPa}$), $3\times$ lower than conventional solutions. However, we will show in Section 3 that this does not adversely affect the performance of the UG.

Concerning the mechanical structure, our modular design approach is shown in Figs. 2 and 4. It consists of three larger sub-assemblies, namely 1. the base, containing the pumps, valves, and controller board, 2. the gripper-floor, forming the interface between the pneumatic system and the detachable membrane module, 3. the membrane module, which itself consists of an interface piece firmly holding onto our custom silicone membrane. It also contains the filter, sealing off the filler material from the environment, while permitting air to circulate freely. The membrane module is held in place by screwing the wedge onto the external printed thread on the gripper-floor. Consequently, the membrane module is pressed against the cast-in-place silicone seal on the gripper-floor, which then forms an air-tight seal. The paper filter has a mechanical support to prevent it from tearing under load.

This modular concept has three main advantages: *first*, it enables quick iteration on membrane module designs; *second*, it allows to quickly and effortlessly swap between different membrane modules during the tests; *third*, it enables the

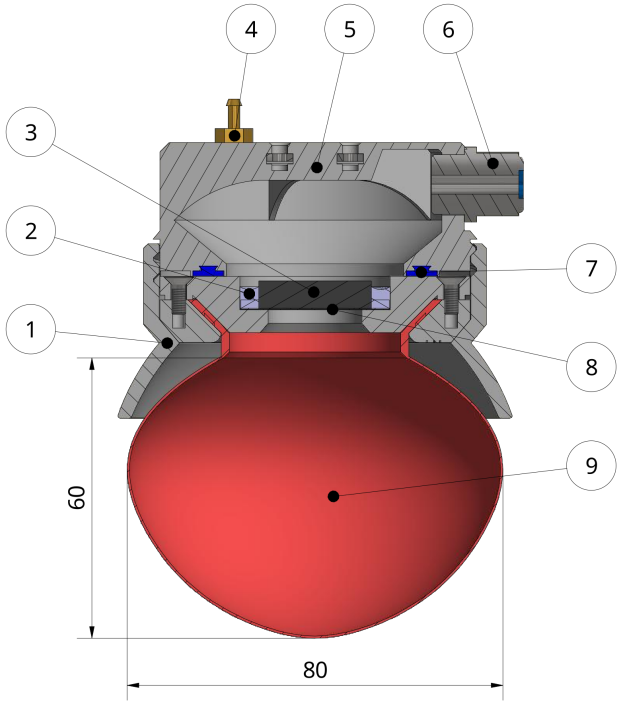

Figure 4: Section view of the main gripping module (membrane module attached to the gripper-floor). ① Wedge with integrated thread, ② Hot-glue seal, ③ Mechanical filter support, ④ Pressure gauge fitting, ⑤ Upper shell, ⑥ Main air inlet/outlet, ⑦ Cast-in-place silicone gasket, ⑧ Paper filter, ⑨ Membrane filled with granular filler material.

platform to be compatible with different types of grippers, given that there are some geometries that cannot be picked up by a UG (e.g., large flat surfaces), which require highly specialized grippers such as vacuum cups.

Our UG is designed to be mounted like a 'claw' on a multirotor, therefore it is designed to do double duty, i.e., to operate as a gripper and also to serve as the landing gear. As such, it is dimensioned to withstand the full weight and impact of a landing UAV, which comes with several advantages that we discuss in Section 6.

2.3 Material Selection

Our membrane is made from the very soft silicone rubber *Trollfactory Type 23*, shore hardness 10 A, $600\,\%$ elongation at break. The reasons for selecting such a soft rubber are twofold: *first*, it allows us to relax the tolerances on the membrane's thickness such that small deviations do not have a big impact on the overall stiffness; *second*, it maximizes the contact area between the membrane and the payload such that the contribution of the friction force is maximized. Furthermore, this particular silicone is meant to be mixed with a silicon additive called *deadener* (also sometimes referred to as *slacker*), which gives the silicone more skin-like physical properties. This further increases the softness of the material, and it also turns it sticky. The intensity of those effects is controlled by the relative amount added to the mixture. This specific silicone rubber is very viscous ($14\,\mathrm{Pa\,s}$) and thus requires particular consideration for the mold design and casting process to avoid trapping air inside the mold and thus creating voids in the thin membrane.

For the printed structural parts, PET-G was chosen over PLA for its higher impact resistance and lower density. Furthermore, PLA is prone to creep under sustained load. The structural parts would not benefit from high-end polymers such as PA6-CF or PEEK as there are no special requirements concerning the stiffness or heat resistance of the material.

Concerning the filler material, we choose EPS beads as this material has a very low density of $17\,\mathrm{kg\,m^{-3}}$, which is - by an order of magnitude - lower than other commonly used materials such as ground coffee or glass beads (Table 1). Moreover, the soft EPS particles develop higher holding forces than rigid particles due to the squeezing effect, which is a result of the elasticity of the EPS beads themselves [17].

Material	Density ($\mathrm{kg\,m^{-3}}$)	Particle Size (mm)
EPS	17	1-4
Coffee	308	0.2-2
Polymer	940	0.1-0.2
Glass	2500	0.2-0.4

Table 1: Comparison of filler materials. EPS has by far the lowest density.

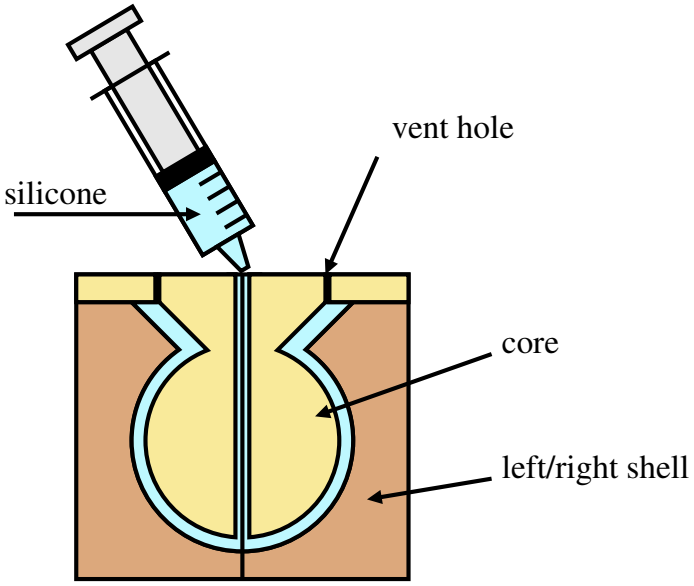

Figure 5: Fabrication process of the membrane. The silicone mixture is injected with a syringe through the mold's core. The air inside the mold escapes through the vent holes at the top. Precise alignment between the shells is critical as the membrane is only $0.6\,\mathrm{mm}$ thick.

2.4 Fabrication

Our membrane is the product of a silicone casting process. We created a three-part mold (i.e., left/right shell and core) printed from PET-G using a common FDM 3D printer. Our approach is similar to [34], however, due to the very thin $0.6\,\mathrm{mm}$ membrane and the high viscosity of the silicone rubber, the process had to be adapted. More precisely, instead of pouring the silicone into the mold, we inject it directly through the core using a syringe (Fig. 5). This technique enables very thin-walled castings (assuming proper alignment of the shells). It allows the silicone mixture to spread evenly with a fairly low risk of catching air bubbles in the process. The usual precautions should be taken when working with silicone, such as proper degassing of the silicone after mixing. Our membrane has a nominal diameter of $80\,\mathrm{mm}$, a nominal thickness of $0.6\,\mathrm{mm}$, a height of $60\,\mathrm{mm}$, an encompassing volume of $0.2\,\mathrm{L}$ and a total mass of only $18\,\mathrm{g}$ (without filler).

The structural parts were also fabricated from PET-G using FDM printing. The resulting parts have proven to be sufficiently airtight using optimal print settings. At the mating point of two structural parts (i.e., ⑤ and ⑨ in Fig. 4), a silicone gasket is introduced that assures an air-tight connection between the two parts.

Our filler material consists of a mixture of Expanded Polystyrene (EPS) beads of various sizes ranging from $1\,\mathrm{mm}$ to $4\,\mathrm{mm}$. Contrary to rigid filler materials such as glass beads, the softness of the particles gives birth to a squeezing effect which is reported to increase the holding force within certain limits [17]. Another consideration for the choice of the filler material was the density and thus the weight of the filled membrane. EPS beads have a very low density of approx. $16.7\,\mathrm{g\,L^{-1}}$ and thus do not add much mass to the system. Other materials such as ground coffee with a density of $308\,\mathrm{g\,L^{-1}}$ or glass beads with $2500\,\mathrm{g\,L^{-1}}$ result in significant extra weight. We added $2.2\,\mathrm{g}$ filler material ($0.13\,\mathrm{L}$) to the membrane corresponding to a fill ratio of $66\,\%$.

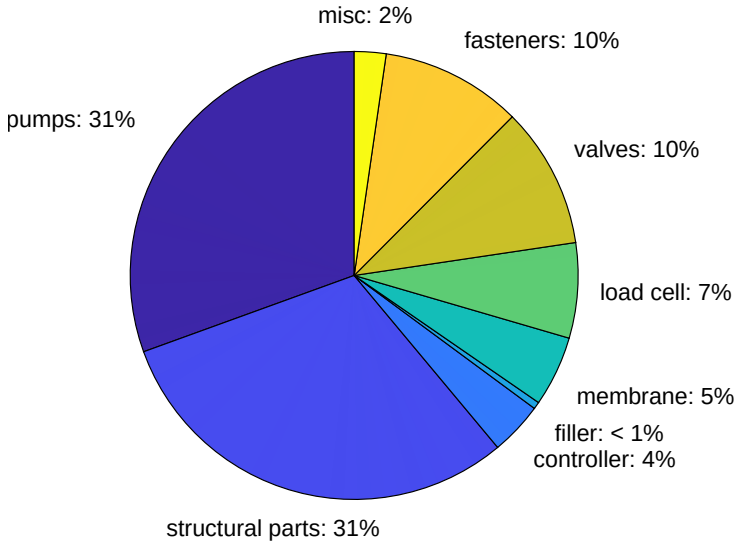

Figure 6: Mass breakdown of the $395\,\mathrm{g}$. The pumps and the structural plastic parts form the bulk of the mass.

The total mass of the assembly ($395\,\mathrm{g}$) is distributed among the different components as shown in Fig. 6. The pneumatic system represents the bulk of the mass ($160\,\mathrm{g}$), followed by the structural plastic parts ($120\,\mathrm{g}$) and the fasteners ($40\,\mathrm{g}$), fittings and tubing (<$8\,\mathrm{g}$). The mass added by the filler material ($2.2\,\mathrm{g}$) is, however, negligible.

2.5 Electronics and Firmware

The system depicted in the block diagram in Fig. 7 is implemented on a single, small, completely custom $47\,\mathrm{mm} \times 47\,\mathrm{mm}$ controller board which is shown in Fig. 2. It is designed to work and integrate easily with common UAV hardware. As such, it can directly be powered by hooking into the main power bus of the drone. Furthermore, it features USB and UART serial ports for communication with an autopilot or an off-board computer.

At the heart of the controller is an ultra-low power STM32L1 microcontroller that does the logic-processing, collection/processing of the sensor data, the communication with the off-board peripherals, and the control of the quad-channel motor driver that powers the pneumatic hardware.

Due to the low power requirements of the controller (less than $50\,\mathrm{mA}$ at $12\,\mathrm{V}$) we have favored linear DC/DC regulators over switching converters due to their inherent complexity and cost. The output stage (valves and pumps) is directly powered by the main power bus. Current chopping ensures that each actuator operates at its nominal operating point regardless of the bus voltage.

The load-cell and the onboard air pressure sensor provide the required data for the system to monitor itself and to work autonomously. In fact, to autopilot, it looks like it is talking to a 'dumb gripper' that only takes open/close commands. We expose however most of the processed sensor readings to enable more advanced applications (e.g., activation force control). We refer to the measured force as F_m, and to the measured pressure as P. This enables applications such as controlling the activation force and also empowers the internal logic to control the pressure inside the membrane and to prevent conditions such as membrane rupture due to over-pressure and to assure a consistent air pressure while approaching the payload.

We define two pressure thresholds, namely $P_{min} = -21\,\mathrm{kPa}$, the lower trigger point, and $P_{max} = 0.5\,\mathrm{kPa}$ the upper trigger point. Those trigger points are used to switch reliably between the 'closed' and 'opened' states of the gripper. In particular, $P \geq P_{max}$ signals that the membrane is full and any additional air would stretch the membrane (consequently increasing the internal pressure). $P \leq P_{min}$, signals that a vacuum is established, and thus the gripper is considered 'closed'.

Internally, the firmware on the MCU is running FreeRTOS, running two tasks using preemptive multitasking as shown in Algorithm 1. Task 1 handles sensors and actuation, and task 2 handles serial communication. Inter-task communication takes place over thread-safe FIFO queues. For the underlying state machine (automaton), we refer the reader to Appendix A. Notice that, for hardware reasons, the controller uses gram-force 'gf' for force measurements.

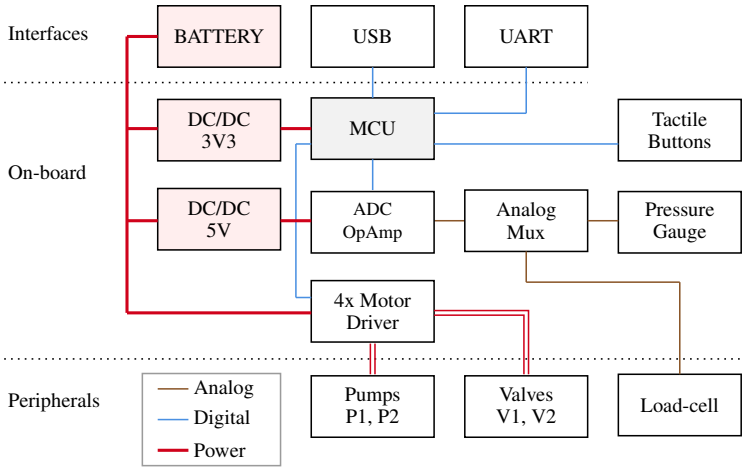

Figure 7: Sensors and control topology. The system features a quad-channel current-chopping motor driver for the pumps P1, P2, and valves V1, V2. The sensors (pressure gauge and load-cell) are interfaced through a multiplexer into a differential operational amplifier + ADC. Communication with the main microcontroller is assured via USB or UART. The power rails are generated from the battery using cascading linear voltage regulators.

Algorithm 1 FreeRTOS, sensor acquisition and actuation

procedure TASK 1: SENSORS AND ACTUATION
  let k_{gr} be the current gripper state
  let $S(k_{gr})$ be the automaton in Fig. 19
  let f_1, f_2 be lowpass FIR filters
  loop
    collect push button states $\mathbf{u_{bt}}$
    fetch raw sensor data P^*, F_m^*
    process sensor data $P \leftarrow f_1(P^*)$, $F_m \leftarrow f_2(F_m^*)$
    create state vector $\mathbf{q} \leftarrow (t, k_{gr}, P, F_m)$
    process automaton $\mathbf{u_a} \leftarrow S(\mathbf{q}, \mathbf{u}))$
    apply $\mathbf{u_a}$ to actuators
  end loop
end procedure
procedure TASK 2: COMMUNICATION
  loop
    outbound communication, send $\mathbf{q}$
    inbound communication, receive $\mathbf{u_{usr}}$
    create command vector $\mathbf{u} \leftarrow (\mathbf{u_{usr}}, \mathbf{u_{bt}})$
  end loop
end procedure

2.6 Grasping Procedure

The UG requires a specific grasping procedure to be followed in order to achieve a successful grasp. Typically this consists of four main steps (Fig. 8):

1. The procedure starts by pushing the gripper against the payload. Doing so will elastically deform the membrane and the filler material will freely flow around the payload. At this point, valves V1 and V2 are still closed such that the free volume remains unchanged. The evacuation phase is then triggered once the measured force reaches the desired activation force F_a, i.e., $F_m \geq F_a$.
2. Evacuating the air out of the membrane. This process takes a couple of seconds (governed by the flow rate of the pumps). During that period, the membrane shrinks, and the contact force drops in response to that. In the context of low activation forces, it is essential to keep good contact with the payload. Failure to do so will lead to a poor or unsuccessful grasp as the filler hardens without properly surrounding the payload. We thus track the nominal activation force during this interval. Other publications in this field usually worked

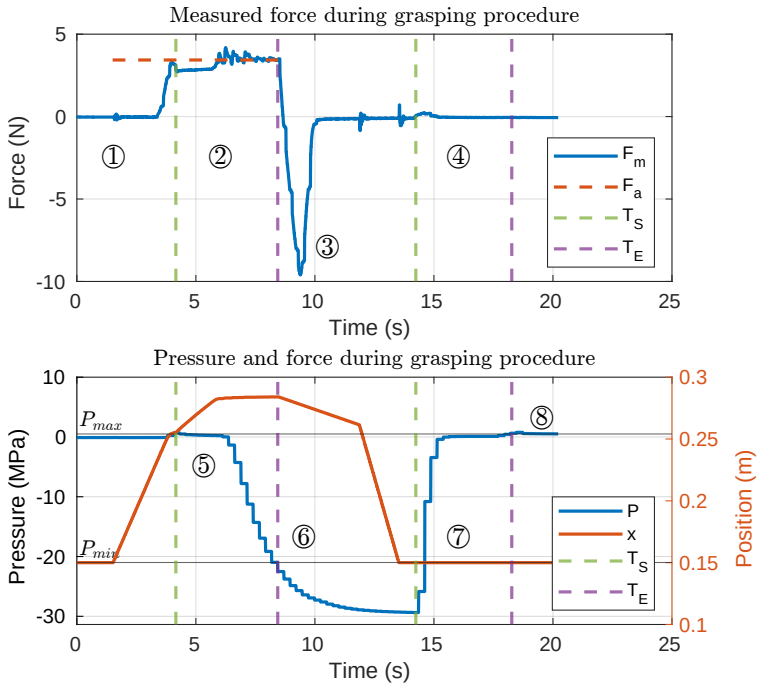

Figure 8: Grasping procedure. ① Approach, ② Evacuation phase where the air is pumped out of the membrane, ③ Retraction phase where the peek marks the maximum holding force, ④ Reset of the gripper by pumping air into the membrane, ⑤ Pressure starts dropping once the volume reaches the minimum, ⑥ End of closing procedure triggered by $P \leq P_{min}$, ⑦ Pressure rises as air is pumped in, ⑧ End of opening procedure triggered by $P \geq P_{max}$. T_S and T_E mark the start and the end of the transition between open and close resp. vise-versa.

around this by pushing the gripper with very significant force into the payload, e.g., [16], which is, however, not possible with aerial systems.

3. Once the membrane's internal pressure P satisfies $P \leq P_{min}$ (vacuum), the grasping procedure is considered completed. The gripper is then retracted from the payload (here, at a constant velocity). Since the payload is fixated to the support and cannot be lifted, a negative force is measured that corresponds to the holding force F_h. In practice, with the gripper mounted on a UAV, instead of the holding force, the actual weight of the lifted payload would be measured, which could be fed back into the autopilot.
4. Releasing the payload (i.e., opening resp. resetting the gripper) is achieved by pumping air into the membrane until $P \geq P_{max}$ is reached, then closing valves V1 and V2. The gripper is now ready to grasp the next object.

The activation force F_a is an important quantity for a successful grasping operation. A too small activation force causes the grasping operation to fail; too high and it damages the force sensor and membrane. In the worst case, it may even cause the UAV to become unstable. Therefore, the optimal activation force has to be chosen as low as possible without sacrificing performance, i.e., without compromising on the maximum holding force.

3 Experiments

In the following sections, we introduce our experimental setup as well as the experiments to, *first*, determine the optimal minimal activation force for the grasping procedure, and *second*, to access the influence of the silicone additive *deadener* on the grasping performance.

We also use this experimental setup to collect data regarding the stiffness of the UG in various states with the goal to create a simple digital twin resp. contact model for common robotics simulators (Section 4).

3.1 Experimental Setup

Our experimental jig used for benchmarking is featured in Fig. 9. It consists of a 12 V supply and a single belt-driven linear rail (capable of fast movements) moving the entire gripper assembly fixated to the horizontal beam. The stepper

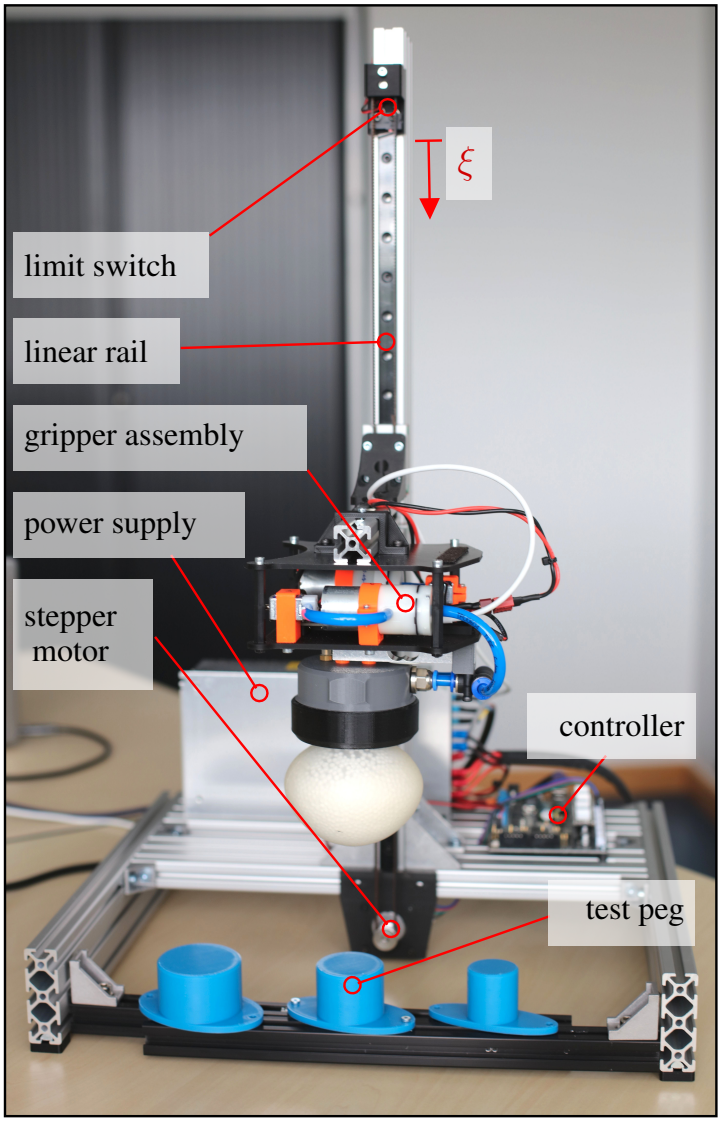

Figure 9: Experimental jig. The UG is attached to a belt-driven linear rail, moving the gripper assembly into contact with the test peg (blue). The test peg is a simple cylindrical object with no features allowing geometric interlocking.

motor is powered and controlled by an off-the-shelf *3D printer board*. The jig does not feature any sensors since they are integrated into the gripper itself.

Velocity commands u_{feed} as well as go-to (position) commands (G-codes) are accepted by our custom firmware on the jig's controller. The current position and velocity are sent back to the host computer for the purpose of logging. Similarly, the gripper's controller sends back its current state and sensor data (force, pressure, and input voltage), while also accepting state transition commands (open resp. close).

Cylindrical test pegs (blue) are representing our payloads. They are fixated at the bottom of the z-axis, such that they cannot be lifted. The pegs are placed such that they are aligned with the center of the membrane. They have no features that would allow for geometric interlocking. As such, the results concerning F_h can be seen as a worst-case scenario.

All of our experiments require tracking of a nominal activation force. As such, given a nominal force F_d and the measured force F_m, we want to drive the error e_f close to zero:

$$e_f = F_d - F_m \tag{1}$$

The input u_{feed} is the commanded linear velocity of the sled. The system itself acts as an integrator since F_m is a function of the position, and as such e_f is guaranteed to be driven close to zero by the simple proportional control law

$$u_{feed} = K_p e_f, \tag{2}$$

where K_p is a positive constant.

3.2 Minimum Activation Force

The activation force is a crucial factor for a successful grasp. However, in the context of aerial manipulation, where the base of the gripper is floating, this becomes an even more important factor as any external forces have the potential to cause stability issues. We would like to point out the following key aspects:

- An aerial platform is severely limited in the amount of force it can apply to its environment before hitting its stability margins.
- The need for a (large) activation force can thus be seen as a net disadvantage of these types of grippers. Reducing it is therefore considered beneficial.

Recent research reported that there is a monotonic relation between the activation force and the resulting holding force [16]. An older study found that after reaching a certain threshold, the holding force stays constant [18]. Our results confirm the findings of both studies and furthermore indicate that this threshold depends on the fill ratio of the membrane.

In this study, we will focus on small activation forces $F_d < 650\,\mathrm{gf}$ as they are the most useful for aerial grasping. We thus conduct six test series with nominal activation forces ranging from $150\,\mathrm{gf}$ to $650\,\mathrm{gf}$ for fill ratios of 66% and 90%. Each test series follows the grasping procedure described in Section 2.6 and is repeated eight times using the $\varnothing 40\,\mathrm{mm}$ peg. For this and all subsequent experiments, we have chosen $K_p = 6$ as a compromise to achieve good force tracking while the membrane is still soft, and to reduce overshoots when the membrane hardens at the end of the evacuation phase.

The results of this study are shown in Figs. 10- 12. The data shows that our gripper can reach a maximum holding force $F_{h,max}$ of about $10\,\mathrm{N}$ for the test peg with $D = \varnothing 40\,\mathrm{mm}$ and without geometric interlocking. The evacuation period typically takes $T_{SE} = T_E - T_S = 4.3\,\mathrm{s}$ (Fig. 8). Furthermore, there is a clear relationship between the fill ratio and the minimal activation forces required to reach the maximal holding force as illustrated in Figs. 11 and 12. Lower fill ratios generally result in lower requirements for the minimum activation force. The gripper with the membrane having the lower fill ratio of 66% reaches $F_{h,max}$ with only a minimal activation force of $250\,\mathrm{gf}$ (see Fig. 11). Increasing the activation force beyond that threshold does not significantly increase the resulting holding force. In case of the higher infill ratio of 90%, $650\,\mathrm{gf}$ are required to get the same holding force (see Fig. 12). Higher fill ratios naturally come with a smaller free volume, i.e., the volume in which the grains can move freely. In turn, the mobility of filler particles is impaired, which manifests in a higher effort to redistribute the filler within the membrane during contact. This manifests itself in a prolonged monotonic relationship between the activation force and the holding force. Therefore the minimum activation force increases with the fill ratio.

We thus conclude that an activation force $F_a \geq 250\,\mathrm{gf}$ is adequate for successful grasping without compromising the holding capability of the gripper. We consider this low enough to work on a wide range of UAVs without significantly impacting the stability of the system. Furthermore, we conclude that lower fill ratios (in the 60% range) are preferable since they require lower activation forces.

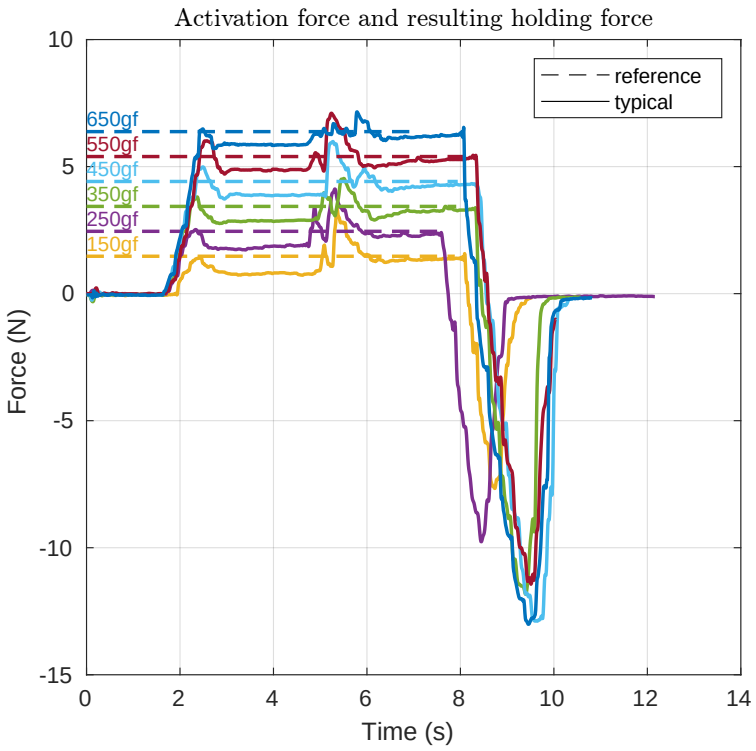

Figure 10: Activation and holding force for various nominal activation forces from 150 gf to 650 gf. The nominal activation force is tracked during the hole evacuation phase (2 s to 8 s). The maximum holding force is then measured during the retraction phase (8 s to 10 s), where it shows up as the peak negative force.

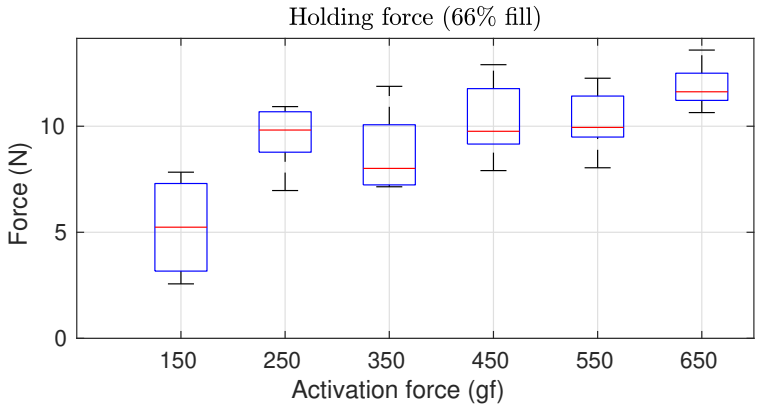

Figure 11: Holding force in relation to the nominal activation force, with a fill ratio of 66 %. The holding force stays constant after reaching the threshold of 250 gf.

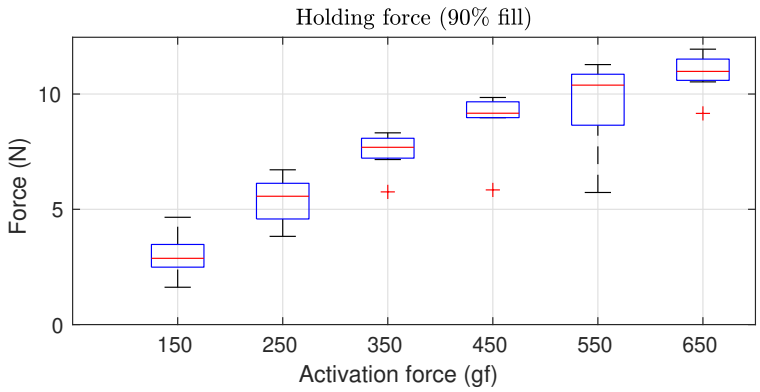

Figure 12: Holding force in relation to the nominal activation force, with a higher fill ratio of 90 %. The holding force increases monotonically with the activation force.

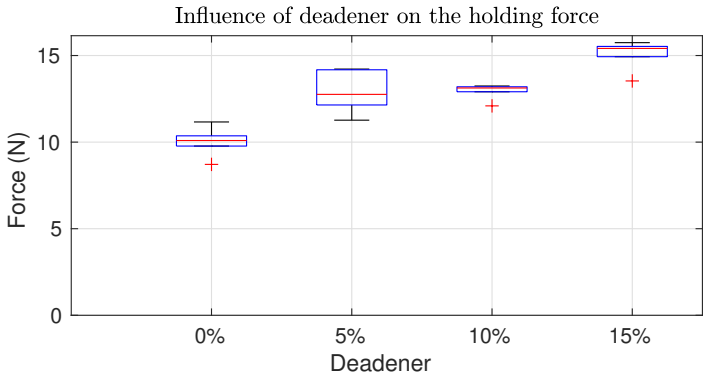

Figure 13: Holding force for various percentages of deadener added to the silicone mixture. Increasing the amount of deadener turns the membrane softer and stickier, increasing the holding force.

3.3 Deadener (Additive)

Deadener (also called *slacker*) is an additive that is added to the silicone during the mixing process. It alters the physical properties of the cured silicone by increasing its softness and stickiness. Both effects can augment the holding force of the developed UG. The former improves the membrane's ability to conform itself to different shapes, and the latter increases the friction between the membrane and the targeted object.

Herein, we measured the effect of adding 0 % to 15 % of deadener (by weight) to the mixture. At around 15 % deadener, the membrane reached a consistency similar to soft chewing gum. Further increasing the percentage was thus deemed impractical.

For the test series, we created four membranes with 0 %, 5 %, 10 % and 15 % deadener. We repeated our holding force test 6 times for each of the membranes, with an activation force of 350 gf, and a test peg of $\varnothing 40$ mm. The results are shown in Fig. 13. Starting with no deadener, we reach the expected holding force of around 10.1 N. A median of 12.8 N and 13.1 N was measured for 5 % and 10 % deadener, respectively. Further increasing it to 15 %, resulting in a median holding force of 15.4 N, a significant increase of 52 % compared to no deadener.

The increase in performance can be explained as follows. On one hand, the additive turns the membrane slightly tacky, thus increasing the friction coefficient between the membrane and the test peg. On the other hand, due to the increased softness, the membrane's ability to conform to the test peg's shape is improved, resulting in a larger contact surface. Both of them cause the contribution of the friction F_R to increase which results in a greater F_H. It should be noted that the stickiness is a temporary effect and dwindles over time as dust or dirt accumulates on the membrane's surface. For a lasting effect, a clean environment is thus required. Alternatively, a periodic replacement/renewal of the membrane module (which is fully supported by our design, see Fig. 2) should be considered.

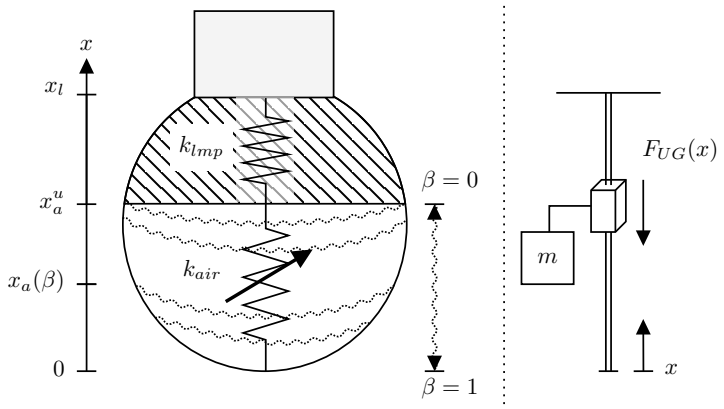

Figure 14: The UG membrane is separated into two components: the air-filled elastic membrane and the rest of the system. Both components are modeled as compression springs k_{air} and k_{lmp} respectively (left). The equivalent mechanical system consists of a prismatic joint with finite travel subjected to the joint force F_{UG} (right).

4 Digital Twin

In the context of aerial manipulation, the UG exhibits challenging dynamic behavior as it transitions from a completely soft state to a jammed (almost rigid) state. This section proposes a homologous model of our gripper based on observations and measurements obtained during our experiments.

Our digital twin will faithfully represent the following main aspects of the UG:

1. the normalized free volume β represented as a first-order system, which models the transition between the membrane's open/closed states.
2. the membrane shrinkage $x_a(\beta)$ caused by the changing free air volume.
3. the contact force contribution of the air-filled membrane represented by the compression spring k_{air} as a function of the payload diameter and the normalized free volume β.
4. the contact force contribution due to the lumped elasticity represented by the compression spring k_{lmp}, which takes into account the complete assembly with the gripper being jammed.

We assume negligible damping, a constant volumetric airflow and $k_{air} \ll k_{lmp}$ and that the membrane does not touch the ground during the grasping phase (satisfied for any reasonably sized payload).

We propose the contact model shown in Fig. 14, consisting of the two non-linear compression springs k_{lmp} and k_{air}, where the latter is of variable stiffness, i.e., dependant on the size of the targeted object. The spring k_{lmp} represents the lumped stiffness of the jammed filler material and the structural parts of the assembly. The spring k_{air} represents the compression of the air-filled membrane during contact. Its stiffness is tied to many parameters such as the effective contact area, the non-linear elastic behavior of the membrane, internal pressure, filled volume, and other factors of which most cannot be measured. Its dynamic behavior is, to some extent, akin to an air spring, e.g., [38]. However, such a precise model is very hard to identify and has no practical benefits in this context.

We employed non-linear regression analysis to identify the relation between the depth of entrance x, the payload/peg diameter $D \in (0; 60]$ (in mm) and the resulting elastic force F_{air} as follows (Fig. 15)

$$F_{air}(x, D) = a_1 D x^{a_2} \tag{3}$$

$$= 102.87 \cdot D x^{1.88}. \tag{4}$$

Similarly, we identified the lumped elastic force of the system to be (Fig. 16)

$$F_{lmp}(x) = a_3 x^{a_4} \tag{5}$$

$$= 25119.75 \cdot x^{1.29}. \tag{6}$$

The combined elastic force F_{ug} is then obtained by

$$F_{ug}(x, D) = F_{air}(H(x), D) + F_l(H(x - x_a)), \tag{7}$$

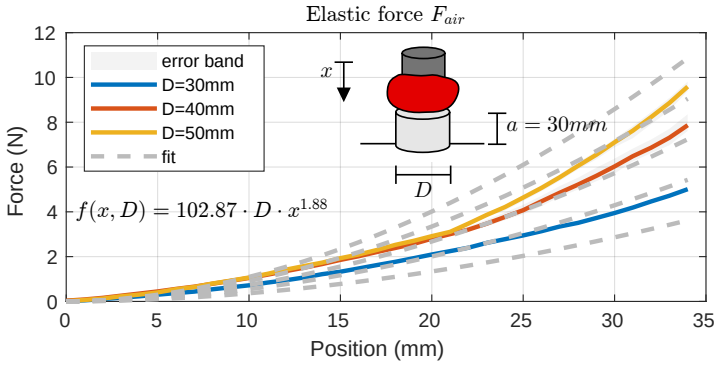

Figure 15: Elastic force F_{air} of the inflated membrane during contact with different sized test pegs from $30\,\mathrm{mm}$ to $50\,\mathrm{mm}$. Larger effective areas generate a higher elastic force.

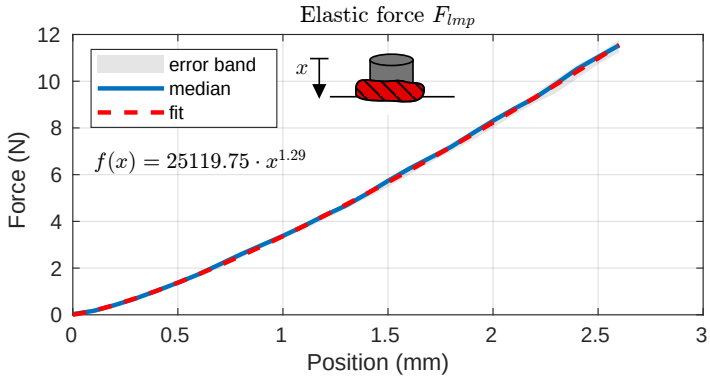

Figure 16: Lumped elastic force F_{lmp} of the jammed membrane-gripper system during contact with the test peg. The diameter of the test peg does not affect the results since the shape of the membrane does not change.

where

$$H(x) = \begin{cases} 0 & \text{if x < 0,} \\ x & \text{if x > 0,} \end{cases} \tag{8}$$

accounts for the fact that the springs act in compression only.

Another key aspect represented by the model is the shrinkage of the membrane during the evacuation phase (see Figs. 8 and 14), where the air is pumped out of the membrane, which consequently shrinks in the process. Herein, it is assumed that this shrinkage follows an exponential law and we designate this internal state by the letter $\beta \in [0; 1]$, where $\beta = 1$ indicates that the membrane is completely filled with air (without stretching it) and $\beta = 0$ means that all the air is evacuated (the filler is jammed resp. in the process of getting jammed). The transition phase is modeled as a first-order system defined as

$$G(s) = \frac{\beta(s)}{R(s)} = \frac{1}{1 + sT}, \tag{9}$$

where $T = 63\,\% \cdot T_{SE} = 2.8\,\mathrm{s}$ is the time constant and $R(s)$ being a unit step (either 0 or 1, depending on the desired state transition). Based on the value of β, we define three discrete gripper states such that

$$k_{gr}(\beta) = \begin{cases} \text{closed} & \text{if } \beta \leq 1\,\% \\ \text{opened} & \text{if } \beta \geq 99\,\% \\ \text{in transition} & \text{otherwise} \end{cases}. \tag{10}$$

Next, we assume (simplify) that the free length x_a^u depends on β as described by the linear mapping

$$x_a(\beta) = x_a^u \cdot \beta, \tag{11}$$

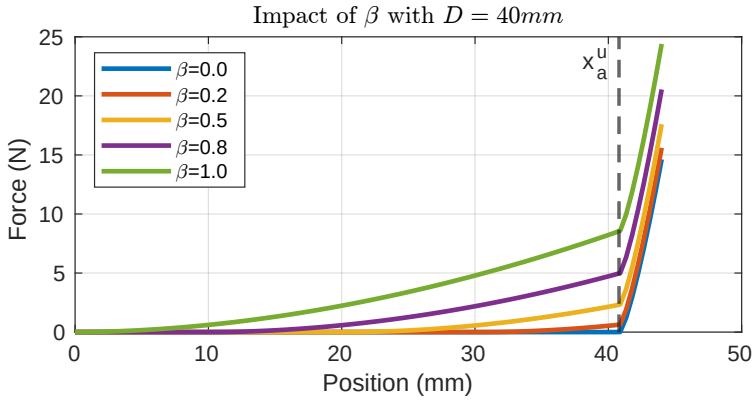

Figure 17: Digital twin's contact force model for different membrane fill ratios from $\beta = 0$ empty/jammed to $\beta = 1$ completely filled with air. The lumped stiffness dominates starting from $x_a^u = 40.8\,\mathrm{mm}$.

where the upper bound x_a^u is defined by the minimal volume occupied by the filler material in the jammed state. Herein, we identified $x_a^u = 40.8\,\mathrm{mm}$ experimentally with it being the position at which the jammed membrane first makes contact with the test peg. We thus conclude with the contact force model as shown in Fig. 17.

As for the grasping part, we suggest considering a grasping procedure to be successful as long as an activation force greater than $250\,\mathrm{gf}$ is maintained with the payload during the entire evacuation phase. A successful grasp should then establish a rigid connection between the gripper and the payload motivated by the jamming (hardening) of the filler material. That connection should be removed if $F_m \geq F_h$ or once the state transition $\beta > \epsilon > 0$, where ϵ is a very small value.

Practical applications of this contact model include estimating the size of the payload with the help of characteristic curves of the elastic forces identified during the initial contact as shown in Fig. 15. This, however, requires precise measurements of the position, which might not be available in real-world conditions.

On the other hand, the contact model is helpful for robotics simulators such as *Gazebo*. We suggest modeling the UG as a point mass of $m = 20\,\mathrm{g}$ (weight of filler plus membrane) attached to a prismatic joint, whose forces F_{UG} are governed by our contact force model (7) and its travel limits are given by the range $[0; x_l]$, where $x_l = 60\,\mathrm{mm}$ is the height of the membrane (see Fig. 14, right). The UG's internal state β is governed by the system model (9).

5 Aerial Application

In this section we briefly present our results concerning the UG attached to a UAV, performing a simple pick and release manipulation task. The overall goal of this experiment is to validate the fundamental concept shown in Fig. 1.

Our proof-of-concept platform based on the frame of the Asctec Firefly features a Raspberry Pi 3 with a Navio 2 running the PX4 autopilot. We created a custom PX4 firmware module to communicate with the gripper and to link one of the remote control channels to trigger its opening resp, closing state transition. Herein, the UAV is carefully manually piloted in position control mode.

The whole experiment is pictured in Fig. 18 and the supplementary video is available online [3]. The procedure of the UAV is to take off, grab the payload (orange), and drop it in the drop-off area. During the setup of the experiment, the UAV is manually placed on the checkerboard. The gripper is then closed via the push buttons on the controller board. This forms a hard and rigid surface for the UAV to rest on. At that stage, the UAV is ready to take off.

After successful takeoff, the membrane of the UG is fluidized (triggered by the remote) and the payload is approached. Ideally, the membrane would hit the payload dead-center, but the UG is fairly tolerant to positional errors. After the activation force crosses a certain threshold, the evacuation phase is automatically triggered and the filler material hardens, giving a firm grasp on the payload. Now, the drone is piloted to the drop-off zone, where it releases its payload by fluidizing the gripper via the remote control.

Lastly, the UAV is piloted back to the checkerboard, where it safely lands on the UG. Notice that the landing gear, although present, never touches the ground and was kept for safety reasons only.

[3] Supplementary video: https://youtu.be/Az5bXnZUNlY

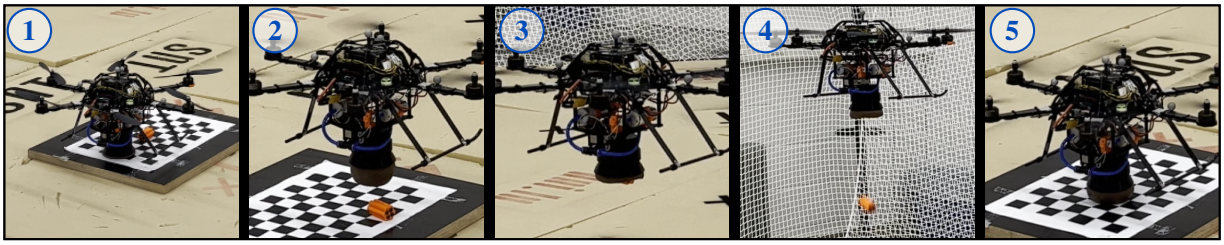

Figure 18: Aerial application. ① The UAV sits on the gripper, ready for takeoff, ② The UAV approaches the payload (orange), ③ After a successful grasp, the UAV departs, ④ Having reached the drop-off area, the payload is released, ⑤ The UAV lands back on the UG.

6 Discussion

The interest in developing soft grippers for aerial vehicles stems from the fact that by leveraging the properties of soft materials, soft grippers are a natural match with dynamic aerial grasping. In contrast to their rigid counterparts, soft grippers are tolerant toward unknown object geometries and surfaces, thus not requiring very high precision. We further advanced the potential of dynamic aerial grasping by developing a lightweight soft jamming universal gripper attached to a UAV. Compared to available soft grippers for aerial grasping, the developed system exhibits several distinguishing characteristics.

First, the developed gripper is highly integrated and modular. The tight integration of the electronics, software, sensors, and mechanics leads to significant weight savings and an overall more defined grasping procedure. The modularity not only helps us to iterate on our design rapidly, but it also addresses some concerns typically associated with UGs. By having a well-defined interface between the grasping part (membrane module) and the supporting hardware, we assured that the membrane is quick and easy (tool-less) to swap in case of damage. In the future, cases that require more specialized grippers (e.g., a suction cup for large flat surfaces) can be addressed by simply creating another module akin to the membrane module presented here. With this work, we introduced the UG as a new type of soft aerial gripper in the field of aerial grasping. Moreover, thanks to the specific characteristics of UG's construction (lightweight filler and membrane), our gripper is particularly well suited for aerial vehicles compared to the typical multi-fingered soft grippers.

Second, our gripper is omnidirectional in contrast to available soft aerial grasping systems, which are sensitive to the object approaching/grasping direction. This relaxes the requirements in terms of gripping accuracy, which are especially advantageous in an aerial context where it increases the platform's grasping capability with regard to a variety of payload properties such as shape, size, material, and geometry. Moreover, in the presented aerial grasping system, the UAV's rotational degrees of freedom are decoupled from the gripper due to its elasticity, while the translational degrees of freedom are soft-coupled to the target object once the gripper enters physical contact. This helps the UAV to stay at the location of the targeted object during the evacuation phase, where it is close to the ground and thus subject to ground effects.

Third, our UG forms a rigid-like flat surface once a vacuum is established and thus enables the UAV to rest on it. This feature makes our manipulating UAV system exceptional as it removes the need for a dedicated landing gear that also often interferes with the attached gripper resp. the sensors required for autonomous grasping. Furthermore, using the UG as landing gear further reduces the weight of our system. On top of that, since the UG is completely soft during the initial contact, it serves as a shock-absorber for the high-speed impact typically associated with landing maneuvers. Besides that, the system is also able - within limits - to compensate for a number of terrain imperfections (e.g., slanted surfaces or small rocks), assuring optimal takeoff and land conditions. Soft finger grippers often cannot guarantee a grasp secure enough to prevent the payload from moving after the initial hold and thus creating further disturbances. Contrary to our UG which, due to the rigidity of the jamming material, forms a system behaving much more akin to a single rigid body.

Forth, hard shocks typically associated with collisions are very challenging both from a mechanical perspective, like the risk of damage, and also from a control perspective (e.g., instability). Passive mechanical compliance alleviates this problem by turning hard socks into soft, elastic impacts. The aspect of passive compliance is especially relevant in aerial manipulation, where the carrying platform is often under-actuated and susceptible to external forces. The developed UG is completely soft during the first contact and thus passively compliant.

7 Conclusion

In this work, we introduced a novel, highly integrated, and lightweight UG with a low activation force for aerial manipulation. We experimentally verified our design and determined the optimal minimum activation force required for our UG to work reliably. We also concluded that the relation between the activation force and the resulting holding force is highly dependent on the fill ratio, i.e., lower fill ratios are preferable since they lower the required activation force. We further investigated possible holding force improvements using a silicone additive (*deadener*), which yielded a $50\,\%$ higher holding force compared to the reference case without deadener.

In the larger context of UGs, we have also shown that high-power pumps are not strictly required for proper grasping operation. On the other hand, the longer cycle times have to be handled properly and failure to do so will result in degraded or even unsuccessful grasps.

Based on our experimental results, we developed a digital twin that faithfully models the most relevant aspects of our UG intended for numerical robotics simulators.

Lastly, we showed preliminary results having the UG attached to a hexacopter, successfully performing a pick and release task under lab conditions.

Future work deals with the activation force control on the real aerial platform during the grasping procedure as well as online path planning adapted to the particularities of the UG in real-world conditions. With regard to the design, we believe that significant weight saving can still be achieved by having some of the structural components to be fabricated out of carbon fiber (e.g., the base plate), which would, however, significantly increase the costs. As a further improvement, the metal fasteners could be replaced by their nylon counterparts since the expected loads are relatively low.

A Automaton

In this appendix, we describe the state machine (automaton) as depicted in Fig. 19. At the beginning (power-up), we assume the state of the gripper to be undefined as it could be either jammed or fluidized. Thus, we start (0) by running a 'startup' cycle which pulls all the air out of the membrane, then refills it until $P > P_{max}$ is reached, then enters the 'opened' state via (1) indicating that the gripper is ready for operation. The transitions (2) and (5) both depend on time and internal pressure. For the closing operation (2) the condition is $P < P_{min}$ or $t > t_{vacc}$. Transition (3) is automatically triggered if $F_m > F_{thr}$ is measured. The opening condition for transition (5) is defined as $P > P_{max}$ or $t > t_{infl}$. The time condition is an additional safety feature in case of sensor malfunction. State transition (4) is typically triggered via user command over the serial port.

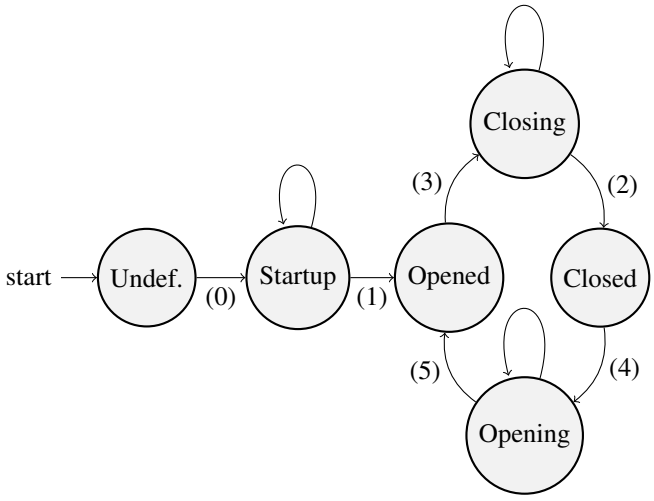

Figure 19: Gripper automaton. The gripper's behavior is governed by the state machine, transitioning between states once certain conditions are met. The main states are 'opened' and 'closed' with intermediary states to handle transitions in between. In the beginning, the state of the gripper is not known, therefore it requires an initial boot procedure. Afterward, the state is well defined by the sensor data.

References

[1] H. A. Almurib, P. T. Nathan, and T. N. Kumar. Control and path planning of quadrotor aerial vehicles for search and rescue. *Proceedings of the SICE Annual Conference*, (2):700–705, 2011.

[2] A. Appius, E. Bauer, M. Blöchlinger, A. Kalra, R. Oberson, A. Raayatsanati, P. Strauch, S. Suresh, M. von Salis, and R. K. Katzschmann. RAPTOR: Rapid Aerial Pickup and Transport of Objects by Robots. pages 1–6, mar 2022.

[3] R. W. Beard, T. W. McLain, D. B. Nelson, D. Kingston, and D. Johanson. Decentralized cooperative aerial surveillance using fixed-wing miniature UAVs. *Proceedings of the IEEE*, 94(7):1306–1323, 2006.

[4] R. P. Behringer and B. Chakraborty. The physics of jamming for granular materials: a review. *Reports on Progress in Physics*, 82(1):012601, jan 2019.

[5] K. Bodie, M. Brunner, M. Pantic, S. Walser, P. Pfndler, U. Angst, R. Siegwart, and J. Nieto. An Omnidirectional Aerial Manipulation Platform for Contact-Based Inspection. In *Robotics: Science and Systems XV*. Robotics: Science and Systems Foundation, jun 2019.

[6] H. Bonyan Khamseh, F. Janabi-Sharifi, and A. Abdessameud. Aerial manipulation—A literature survey. *Robotics and Autonomous Systems*, 107:221–235, 2018.

[7] E. Brown, N. Rodenberg, J. Amend, A. Mozeika, E. Steltz, M. R. Zakin, H. Lipson, and H. M. Jaeger. Universal robotic gripper based on the jamming of granular material. *Proceedings of the National Academy of Sciences*, 107(44):18809–18814, nov 2010.

[8] D. W. Casbeer, D. B. Kingston, R. W. Beard, and T. W. Mc lain. Cooperative forest fire surveillance using a team of small unmanned air vehicles. *International Journal of Systems Science*, 37(6):351–360, may 2006.

[9] Z. Chen, H. Rahimi Nohooji, and C.-M. Chew. Development of Topology Optimized Bending-Twisting Soft Finger. *Journal of Mechanisms and Robotics*, 14(5):1–23, oct 2022.

[10] M. T. Connolly. The Use of Multi Rotor Remotely Operated Aerial Vehicles ROAVs as a Method of Close Visually Inspecting CVI Live and Difficult to Access Assets on Offshore Platforms. In *Day 1 Mon, November 10, 2014*, volume 6, pages 4788–4801. SPE, nov 2014.

[11] B. S. Faiçal, F. G. Costa, G. Pessin, J. Ueyama, H. Freitas, A. Colombo, P. H. Fini, L. Villas, F. S. Osório, P. A. Vargas, and T. Braun. The use of unmanned aerial vehicles and wireless sensor networks for spraying pesticides. *Journal of Systems Architecture*, 60(4):393–404, apr 2014.

[12] J. Fishman and L. Carlone. Control and Trajectory Optimization for Soft Aerial Manipulation. *IEEE Aerospace Conference Proceedings*, 2021-March, 2021.

[13] J. Fishman, S. Ubellacker, N. Hughes, and L. Carlone. Dynamic Grasping with a "Soft" Drone: From Theory to Practice. In *2021 IEEE/RSJ International Conference on Intelligent Robots and Systems (IROS)*, pages 4214–4221. IEEE, sep 2021.

[14] J. Fishman, S. Ubellacker, N. Hughes, and L. Carlone. Dynamic Grasping with a "Soft" Drone: From Theory to Practice. In *2021 IEEE/RSJ International Conference on Intelligent Robots and Systems (IROS)*, pages 4214–4221. IEEE, sep 2021.

[15] F. J. Garcia Rubiales, P. Ramon Soria, B. C. Arrue, and A. Ollero. Soft-Tentacle Gripper for Pipe Crawling to Inspect Industrial Facilities Using UAVs. *Sensors*, 21(12):4142, jun 2021.

[16] J. M. Gómez–Paccapelo, A. A. Santarossa, H. D. Bustos, and L. A. Pugnaloni. Effect of the granular material on the maximum holding force of a granular gripper. *Granular Matter*, 23(1):1–6, 2021.

[17] H. Götz, A. Santarossa, A. Sack, T. Pöschel, and P. Müller. Soft particles reinforce robotic grippers: robotic grippers based on granular jamming of soft particles. *Granular Matter*, 24(1):31, feb 2022.

[18] J. Kapadia and M. Yim. Design and performance of nubbed fluidizing jamming grippers. In *2012 IEEE International Conference on Robotics and Automation*, number 3, pages 5301–5306. IEEE, may 2012.

[19] F. Käslin, T. Baur, P. Meier, P. Koller, N. Buchmann, P. D'Odorico, and W. Eugster. Novel Twig Sampling Method by Unmanned Aerial Vehicle (UAV). *Frontiers in Forests and Global Change*, 1(October), oct 2018.

[20] C. C. Kessens, J. Thomas, J. P. Desai, and V. Kumar. Versatile aerial grasping using self-sealing suction. In *2016 IEEE International Conference on Robotics and Automation (ICRA)*, volume 2016-June, pages 3249–3254. IEEE, may 2016.

[21] Y. Kim and Y. Cha. Soft Pneumatic Gripper With a Tendon-Driven Soft Origami Pump. *Frontiers in Bioengineering and Biotechnology*, 8(May):1–11, 2020.

[22] P. Kremer, J. L. Sanchez-Lopez, and H. Voos. A Hybrid Modelling Approach for Aerial Manipulators. *Journal of Intelligent & Robotic Systems*, 105(4):74, aug 2022.

[23] L. Kruse and J. Bradley. A Hybrid, Actively Compliant Manipulator/Gripper for Aerial Manipulation with a Multicopter. In *2018 IEEE International Symposium on Safety, Security, and Rescue Robotics (SSRR)*, pages 1–8. IEEE, aug 2018.

[24] H. Li, B. Wang, L. Liu, G. Tian, T. Zheng, and J. Zhang. The design and application of SmartCopter: An unmanned helicopter based robot for transmission line inspection. In *2013 Chinese Automation Congress*, pages 697–702. IEEE, nov 2013.

[25] S. Li, J. J. Stampfli, H. J. Xu, E. Malkin, E. V. Diaz, D. Rus, and R. J. Wood. A Vacuum-driven Origami "Magic-ball" Soft Gripper. In *2019 International Conference on Robotics and Automation (ICRA)*, pages 7401–7408. IEEE, may 2019.

[26] S. Licht, E. Collins, D. Ballat-Durand, and M. Lopes-Mendes. Universal jamming grippers for deep-sea manipulation. In *OCEANS 2016 MTS/IEEE Monterey*, pages 1–5. IEEE, sep 2016.

[27] G. Loianno and V. Kumar. Cooperative transportation using small quadrotors using monocular vision and inertial sensing. *IEEE Robotics and Automation Letters*, 3(2):680–687, 2018.

[28] A. McLaren, Z. Fitzgerald, G. Gao, and M. Liarokapis. A Passive Closing, Tendon Driven, Adaptive Robot Hand for Ultra-Fast, Aerial Grasping and Perching. In *IEEE International Conference on Intelligent Robots and Systems*, pages 5602–5607. IEEE, nov 2019.

[29] S. Mishra, D. Yang, C. Thalman, P. Polygerinos, and W. Zhang. Design and Control of a Hexacopter With Soft Grasper for Autonomous Object Detection and Grasping. In *Dynamic Systems and Control Conference*, number September, page V003T36A003. American Society of Mechanical Engineers, sep 2018.

[30] J. Moore and R. Tedrake. Powerline Perching with a Fixed-Wing UAV. In *AIAA Infotech@Aerospace Conference*, number April, Reston, Virigina, apr 2009. American Institute of Aeronautics and Astronautics.

[31] T. Nishida, Y. Okatani, and K. Tadakuma. Development of Universal Robot Gripper Using MRα Fluid. *International Journal of Humanoid Robotics*, 13(04):1650017, dec 2016.

[32] J.-P. Ore, S. Elbaum, A. Burgin, and C. Detweiler. Autonomous Aerial Water Sampling. *Journal of Field Robotics*, 32(8):1095–1113, dec 2015.

[33] K. M. Popek, M. S. Johannes, K. C. Wolfe, R. A. Hegeman, J. M. Hatch, J. L. Moore, K. D. Katyal, B. Y. Yeh, and R. J. Bamberger. Autonomous Grasping Robotic Aerial System for Perching (AGRASP). In *2018 IEEE/RSJ International Conference on Intelligent Robots and Systems (IROS)*, pages 1–9. IEEE, oct 2018.

[34] T. Sakuma, F. Von Drigalski, M. Ding, J. Takamatsu, and T. Ogasawara. A Universal Gripper Using Optical Sensing to Acquire Tactile Information and Membrane Deformation. *IEEE International Conference on Intelligent Robots and Systems*, pages 6431–6436, 2018.

[35] J. Shintake, V. Cacucciolo, D. Floreano, and H. Shea. Soft Robotic Grippers. *Advanced Materials*, 30(29), 2018.

[36] A. Shukla and H. Karki. Application of robotics in onshore oil and gas industry-A review Part i. *Robotics and Autonomous Systems*, 75:490–507, 2016.

[37] C. A. Thiels, J. M. Aho, S. P. Zietlow, and D. H. Jenkins. Use of unmanned aerial vehicles for medical product transport. *Air Medical Journal*, 34(2):104–108, 2015.

[38] H. Zhu, J. Yang, Y. Zhang, X. Feng, and Z. Ma. Nonlinear dynamic model of air spring with a damper for vehicle ride comfort. *Nonlinear Dynamics*, 89(2):1545–1568, jul 2017.